Interaction and Multiscale Mechanics, Vol. 5, No. 2 (2012) 131-144
DOI: http://dx.doi.org/10.12989/imm.2012.5.2.131

Radial basis function collocation method for a rotating Bose-Einstein condensation with vortex lattices

Y.T. Shih*, C.C. Tsai and K.T. Chen

Department of Applied Mathematics, National Chung Hsing University, Taichung 40227, Taiwan

(Received November 30, 2011, Revised April 15, 2012, Accepted April 16, 2012)

Abstract. We study a radial basis function collocation method (RBFCM) to discretize a coupled nonlinear Schrödinger equation (CNLSE) that governs a two dimensional rotating Bose-Einstein condensate (BEC) with an angular momentum rotation term. We exploit a RBFCM-continuation method (RBFCM-CM) to trace the solution curve of the CNLSE. We compare the performance of the RBFCM-CM with the FEM-CM. We observe that the RBFCM-CM is very robust in a coarse grid for resolving the ground state solution with many vortices when the angular momentum rotation is close to the limit. Numerical results demonstrate the efficiency and accuracy of the RBFCM-CM for computing the superfluid density of the ground level of the BEC.

Keywords: radial basis collocation; inverse multiquadric; meshless; rotating bec; continuation method; vortex lattice; nonlinear schrödinger equation.

1. Introduction

Bose-Einstein condensation (BEC), the phenomenon that clouds of weakly interacting alkali-metal atoms occupy a single quantum state, can be described by a macroscopic wavefunction below a critical temperature T_c. Many researchers in physics or mathematics have been interested in simulating the model problem since the gaseous BEC was experimentally observed in 1995 (Anderson 1995, Davis 1995). When a BEC undergoes a rotating frame, it won't rotate due to its superfluid property of irrotationality. Instead, a vortex lattice will form with each vortex carries the angular momentum (Butts 1999, Rosenbuch 2002).

Many theoretical analysis and numerical computation have been done for the rotating BEC. Bao *et al*. (2006) proposed a time-splitting pseudo spectral method for rotating BEC. Chang and Chien (2007) used the finite difference-continuation method to trace the solution branches of rotating BEC. Baksmaty (2009) described a finite element numerical approach to the full Hartree-Fock-Bogoliubov treatment of a vortex lattice in a rapidly rotating BEC. Matveenko (2009) presented an analytical solution for the vortex lattice in a rapidly rotating BEC in the lowest Landau level.

The radial basis function (RBF) was introduced by Hardy (1971) for interpolating smooth functions. Kansa (1992) used the RBFs to approximate the function and its partial derivative for

* Corresponding author, Associate Professor, E-mail: yintzer_shih@email.nchu.edu.tw

solving the partial differential equations (PDEs). Since then this method has been extensively and widely applied to various linear and nonlinear PDE problems via the collocation method (CM) (Fasshauer 2002, Ferreira 2005, Hu *et al*. 2005, Fornberg 2008, Wang *et al*. 2009, Kindelan 2010). Hu *et al*. (2009) presented the reproducing kernel collocation method (RKCM) to prevent the ill-conditioned system matrix. However, to our knowledge to solve a rotating BEC or any eigenvalue problem by using the RBFCM has not been implemented in the published literature. In this paper, we simulate the phenomenon of the rotating BEC numerically via the RBFCM-continuation methd (RBFCM-CM) to evaluate its superfluid density.

This paper is organized as follows. In Section 2, we briefly review a model problem for a rotating BEC. In Section 3, we formulate the discrete nonlinear system of equations by the RBFCM, and the residual vector functions will be used for in the continuation method to trace the solution curve. Numerical results for the linear Schrödinger equation (LSE) and a coupled nonlinear Schrödinger equation (CNLSE) are reported in Section 4. Finally, some concluding remarks are given in Section 5.

2. A model problem for rotating BEC

The rotating BEC around z-axis at the temperature much smaller than the critical temperature, is modeled by a time dependent nonlinear Schrödinger equation (NLSE), or called the well-known Gross-Pitaevskii equation (GPE) with an angular momentum rotational term (Gross and Pitaevskii 1961) as follows

$$\begin{cases} i\Psi_t(\hat{\mathbf{x}}, t) = -\frac{1}{2}\Delta\Psi(\hat{\mathbf{x}}, t) + V(\hat{\mathbf{x}})\Psi + \mu|\Psi|^2\Psi(\hat{\mathbf{x}}, t) - \omega L_z\Psi(\hat{\mathbf{x}}, t) & t \in (0, \infty), \hat{\mathbf{x}} \in \hat{\Omega}, \\ \Psi(\hat{\mathbf{x}}, t) = 0 & t \in [0, \infty), \hat{\mathbf{x}} \in \partial\hat{\Omega}, \end{cases} \tag{1}$$

where $\hat{\mathbf{x}} = (x, y, z) \in \hat{\Omega} \subset \mathbb{R}^3$ is a bounded domain with a piecewise smooth boundary $\partial\hat{\Omega}$, $\Psi(\hat{\mathbf{x}}, t)$ the macroscopic wave function, μ the intra-component scattering length

$$V(\hat{\mathbf{x}}) = \frac{1}{2}(\gamma_x{}^2x^2 + \gamma_y{}^2y^2 + \gamma_z{}^2z^2)$$

the trapping potential for constants γ_x, γ_y and γ_z with respect to x-, y- and z-directions, an angular velocity ω and the z-component of the angular momentum $L_z = -i(x\partial y - y\partial x)$, where the mass conservation constraint of wave function satisfies

$$\int_{\hat{\Omega}} |\Psi(\hat{\mathbf{x}}, t)|^2 d\hat{\mathbf{x}} = 1 \qquad \text{for all } t \geq 0. \tag{2}$$

Let $\Psi(\hat{\mathbf{x}}, t) = e^{-i\lambda t}q(\hat{\mathbf{x}})$, where $q(\hat{\mathbf{x}})$ is a complex function and λ is the chemical potential. Under the assumption that γ_z is much greater than γ_x and γ_y, and following Chang and Chien (2007) the time-independent GPE turns into a two dimensional coupled nonlinear Schrödinger eigenvalue problem (CNLSE) as follows

$$\begin{cases} -\frac{1}{2}\Delta u(\mathbf{x}) + V(\mathbf{x})u(\mathbf{x}) + \mu|q(\mathbf{x})|^2 u(\mathbf{x}) - \omega(x\partial y - y\partial x)v(\mathbf{x}) = \lambda u(\mathbf{x}) & \mathbf{x} \in \Omega, \\ -\frac{1}{2}\Delta v(\mathbf{x}) + V(\mathbf{x})v(\mathbf{x}) + \mu|q(\mathbf{x})|^2 v(\mathbf{x}) + \omega(x\partial y - y\partial x)u(\mathbf{x}) = \lambda v(\mathbf{x}) & \mathbf{x} \in \Omega, \\ u(\mathbf{x}) = v(\mathbf{x}) = 0 & \mathbf{x} \in \partial\Omega, \end{cases} \tag{3}$$

with the mass conservation constraint

$$\int_\Omega |q(\mathbf{x})|^2 d\mathbf{x} = 1 \tag{4}$$

where the bounded domain $\Omega \subset \mathbb{R}^2$, $\mathbf{x} = (x, y)$.

3. The RBFCM-continuation method (RBFCM-CM) for CNLSE

In this section, we consider the RBFCM for the discretization of the CNLSE, and then use a continuation algorithm to trace the solution curve. To begin with, we consider the linearized Schrödinger eigenvalue problem (LSE)

$$\begin{cases} -\frac{1}{2}\Delta u(\mathbf{x}) + V(\mathbf{x})u(\mathbf{x}) = \lambda u(\mathbf{x}) & \mathbf{x} \in \Omega = (-l, l)^2, \\ u(\mathbf{x}) = 0 & \mathbf{x} \in \partial\Omega. \end{cases} \tag{5}$$

Following the RBFCM of Kansa (1992), the approximate solution u^h is a linear combination of the RBFs given by

$$u^h(\mathbf{x}) \cong \sum_{i=1}^{N} a_i g_i(\mathbf{x}) \tag{6}$$

where $g_i \in C^2(\Omega) \cap C(\partial\Omega)$ is the RBF N is the number of the RBFs in $\Omega \cup \partial\Omega$ and a_i the coefficient of the RBFs. Throughout this paper, we use inverse multiquadrics (IMQ) to be the RBF defined by

$$g_i(\mathbf{x}) = \frac{1}{\sqrt{(x - x_i)^2 + (y - y_i)^2 + c^2}} \tag{7}$$

where (x_i, y_i) are source points of the RBFs and $c > 0$ is the shape parameter. Note that the IMQ is in $C^\infty(\Omega)$.

Let N^i be the total number of interior collocation points $\{x_{I_j} \in \Omega\}_{j=1}^{N^i}$ and N^b the total number of boundary collocation points $\{x_{B_j} \in \partial\Omega\}_{j=1}^{N^b}$. When $N^i + N^b = N$, the discretized algebraic system is linear. Micchelli (1986) shows that for the RBFs by IMQ with constant shape parameter, the matrix

of the system is strictly positive definite. Thus the discrete linear system has a unique solution. And when $N^i + N^b > N$, the coefficients can be obtained by the least square method to minimize the approximation error. Hence if the number of given collocation points is more than the number of source points, then one can achieve an accurate solution for solving a simple elliptic problem (e.g. Hu *et al*. 2005). However, when solving the eigenvalue value problem by a continuation method, it requires an additional small perturbation for tracing the solution branch. Thus, when $N^i + N^b > N$, a mixture of the RBFCM with the minimum processing and the continuation algorithm might cause an irreconcilable conflict and it brings some difficulty for tracing the solution curve. Hence, in this paper we use a traditional RBFCM, i.e., the collocation points are the same as the source points.

Subject all interior collocation points to Eq. (7), and it leads to

$$\mathbf{u} \cong \mathbf{G} \cdot \mathbf{a} \tag{8}$$

where $\mathbf{u} = [u(\mathbf{x}_{I_1}), u(\mathbf{x}_{I_2}), \ldots, u(\mathbf{x}_{I_{N^i}})]^T$, $\mathbf{G}$ is a $N^i \times N$ matrix with entries $G_{ji} = g_i(\mathbf{x}_{I_j})$, for $1 \le i \le N$, $1 \le j \le N^i$, and the coefficient vector $\mathbf{a} = [a_1, a_2, ..., a_N]^T$. Let $\mathbf{D}$,$\mathbf{V}$ be $N^i \times N$ matrices with entries

$$\mathbf{D}_{ji} = -\frac{1}{2}\Delta g_i(\mathbf{x}_{I_j}), \quad \mathbf{V}_{ji} = V(\mathbf{x}_{I_j}) g_i(\mathbf{x}_{I_j}) \quad 1 \le i \le N, \quad 1 \le j \le N^i.$$

Thus, following the collocation method methodology we have

$$\mathbf{P} \cong \mathbf{D} \cdot \mathbf{a}, \quad \mathbf{C} \cong \mathbf{V} \cdot \mathbf{a}, \tag{9}$$

the approximations for

$$\mathbf{P} = -\frac{1}{2}[\Delta u(\mathbf{x}_{I_1}), \Delta u(\mathbf{x}_{I_2}), \ldots, \Delta u(\mathbf{x}_{I_{N^i}})]^T,$$

$$\mathbf{C} = [V(\mathbf{x}_{I_1})u(\mathbf{x}_{I_1}), V(\mathbf{x}_{I_2})u(\mathbf{x}_{I_2}), \ldots, V(\mathbf{x}_{I_{N^i}})u(\mathbf{x}_{I_{N^i}})]^T.$$

The boundary condition leads to

$$\mathbf{u}^b \cong \mathbf{B} \cdot \mathbf{a} = \mathbf{0}$$

where $\mathbf{B}$ is a $N^b \times N$ matrix with entries

$$B_{ji} = g_i(\mathbf{x}_{B_j}), \quad 1 \le i \le N, \quad 1 \le j \le N^b.$$

Hence we use the RBFCM to discretize Eq. (5) as follows

$$\begin{bmatrix} \mathbf{D} + \mathbf{V} \\ \mathbf{B} \end{bmatrix} \cdot \mathbf{a} = \begin{bmatrix} \lambda \mathbf{G} \\ \mathbf{0} \end{bmatrix} \cdot \mathbf{a}. \tag{10}$$

Next we implement a predictor-corrector continuation algorithm (Allgower 1990) to solve Eq. (10). Re-write Eq. (10) by defining the vector function

$$\mathbf{H}(\mathbf{a}, \lambda) = \begin{bmatrix} (\mathbf{D} + \mathbf{V}) \cdot \mathbf{a} - \lambda \mathbf{G} \cdot \mathbf{a} \\ \mathbf{B} \cdot \mathbf{a} \end{bmatrix} = \mathbf{0}. \tag{11}$$

Let $\mathbf{p}(\mathbf{s}^{(i)}) = \mathbf{p}^{(i)} = (\mathbf{a}^{(i)}, \lambda^{(i)}) \in \mathbb{R}^{N+1}$ be an accepted approximating point for the solution curve $\mathbf{C}(s)$ at the parameter $\mathbf{s} = \mathbf{s}^{(i)}$ for Eq. (11). The Euler predictor is defined by

$$\mathbf{p}_0^{(i)} = \mathbf{p}^{(i)} + \delta^{(i)}\mathbf{t}^{(i)} \tag{12}$$

where $\delta^{(i)}$ is the step size, and $\mathbf{t}^{(i)} \in \mathbb{R}^{N+1}$ the unit tangent vector at $\mathbf{p}^{(i)}$ is obtained by solving

$$\hat{\mathbf{A}}(\mathbf{p}^{(i)}) \cdot \mathbf{t}^{(i)} = \begin{bmatrix} \mathbf{0} \\ \mathbf{1} \end{bmatrix}$$

where

$$\hat{\mathbf{A}}(\mathbf{p}^{(i)}) = \begin{bmatrix} [D_{\mathbf{a}}\mathbf{H}(\mathbf{p}^{(i)}) \; D_{\lambda}\mathbf{H}(\mathbf{p}^{(i)})] \\ [\mathbf{t}^{(i-1)}]^T \end{bmatrix} = \begin{bmatrix} \begin{bmatrix} \mathbf{D} + \mathbf{V} - \lambda^{(i)}\mathbf{G} & -\mathbf{G} \cdot \mathbf{a}^{(i)} \\ \mathbf{B} & \mathbf{0} \end{bmatrix} \\ [\mathbf{t}^{(i-1)}]^T \end{bmatrix}.$$

To keep the orientation and to control the local curve, we impose the constraint $\mathbf{t}^{(i)} \cdot \mathbf{t}^{(i-1)} = 1 - \alpha > 0$ for some $\alpha \in (0, 1)$.

Next, the corrector step is performed to improve the accuracy of the predicted point. The Newton iteration is as follows

$$\mathbf{p}_k^{(i)} = \mathbf{p}_{k-1}^{(i)} + \Delta\mathbf{p}_k^{(i)}, \quad \text{for } k = 1, 2, \ldots, \tag{13}$$

where $\Delta\mathbf{p}_k^{(i)}$ is obtained by solving

$$\hat{\mathbf{A}}(\mathbf{p}_{k-1}^{(i)}) \cdot \Delta\mathbf{p}_k^{(i)} = \begin{bmatrix} -\mathbf{H}(\mathbf{p}_k^{(i)}) \\ 0 \end{bmatrix} = \begin{bmatrix} -(\mathbf{D} + \mathbf{V} - \lambda_k^{(i)}\mathbf{G}) \cdot \mathbf{a}_k^{(i)} \\ 0 \end{bmatrix}.$$

If $p_0^{(i)}$ is close enough to the solution curve, then $p_k^{(i)}$ will converge to an approximating point on the solution curve $\mathbf{C}(s)$ for $s = s_{i+1}$. Then we set $\mathbf{p}^{(i+1)} = \mathbf{p}_k^{(i)}$.

For the CNLSE (3), let the approximation of $u(\mathbf{x})$ and $v(\mathbf{x})$ be given by $u^h(\mathbf{x}) = \Sigma_{i=1}^{N} a_i g_i(\mathbf{x})$ and $v^h(\mathbf{x}) = \Sigma_{i=1}^{N} b_i g_i(\mathbf{x})$, respectively. The RBFCM approximation of Eq. (3) is written as

$$\begin{cases} (\mathbf{D} + \mathbf{V}) \cdot \mathbf{a} + \mathbf{E} + \mathbf{L} = \lambda\mathbf{G} \cdot \mathbf{a} \\ (\mathbf{D} + \mathbf{V}) \cdot \mathbf{b} + \mathbf{K} + \mathbf{Q} = \lambda\mathbf{G} \cdot \mathbf{b} \\ \mathbf{B} \cdot \mathbf{a} = \mathbf{0} \\ \mathbf{B} \cdot \mathbf{a} = \mathbf{0} \end{cases} \tag{14}$$

where the coefficient vectors $\mathbf{a}$ and $\mathbf{b} = [b_1, b_2, \ldots, b_N]^T$ for $u(x)$ and $v(x)$, respectively, and the vector functions $\mathbf{E}$, $\mathbf{K}$, $\mathbf{L}$, $\mathbf{Q}$ with entries

$$\mathbf{E}_j = u^3(\mathbf{x}_{I_j}) + v^2(\mathbf{x}_{I_j})\, u(\mathbf{x}_{I_j}), \quad \mathbf{K}j = v^3(\mathbf{x}_{I_j}) + u^2(\mathbf{x}_{I_j})\, v(\mathbf{x}_{I_j}),$$

$$\mathbf{L}_j = -\omega(x_{I_j}\, v(\mathbf{x}_{I_j}) - y_{I_j}\, v(\mathbf{x}_{I_j})), \quad \mathbf{Q}_j = \omega(x_{I_j}\, u(\mathbf{x}_{I_j}) - y_{I_j}\, u(\mathbf{x}_{I_j})),$$

for interior point $\mathbf{x}_{I_j} = (x_{I_j}, y_{I_j})$, $1 \le j \le N^i$. Next consider the continuation method for the nonlinear vector function Eq. (14) as

$$\mathbf{F}(\mathbf{a}, \mathbf{b}, \lambda) = \begin{bmatrix} (\mathbf{D} + \mathbf{V} - \lambda\mathbf{G}) \cdot \mathbf{a} + \mathbf{E} + \mathbf{L} \\ (\mathbf{D} + \mathbf{V} - \lambda\mathbf{G}) \cdot \mathbf{b} + \mathbf{K} + \mathbf{Q} \\ \mathbf{B} \cdot \mathbf{a} \\ \mathbf{B} \cdot \mathbf{b} \end{bmatrix} = \mathbf{0}. \tag{15}$$

To trace a nontrivial solution, a small perturbation vector $\mathbf{d}$ is added to Eq. (15), and we get

$$\tilde{\mathbf{F}}(\mathbf{a}, \mathbf{b}, \lambda) = \mathbf{F}(\mathbf{a}, \mathbf{b}, \lambda) + \mathbf{d} = 0 \tag{16}$$

which is the perturbation for the discretzation equation for rotating BEC. Let $\mathbf{z}(\mathbf{s}^{(i)}) = \mathbf{z}^{(i)} = (\mathbf{a}^{(i)}, \mathbf{b}^{(i)}, \lambda^{(i)}) \in \mathbb{R}^{2N+1}$ be an accepted approximating point on the solution curve $\mathbf{C}$ for Eq. (16). The predict-corrector continuation algorithm is employed to solve the equation. Define the Euler predictor

$$\mathbf{z}_0^{(i)} = \mathbf{z}^{(i)} + \delta^{(i)}\, \mathbf{t}^{(i)} \tag{17}$$

where $\delta^{(i)}$ is the step size, and $\mathbf{t}^{(i)} \in \mathbb{R}^{2N+1}$ the unit tangent vector at point $\mathbf{z}^{(i)}$ solved by

$$\hat{\mathbf{A}}(\mathbf{z}^{(i)}) \cdot \mathbf{t}^{(i)} = \begin{bmatrix} \mathbf{0} \\ 1 \end{bmatrix} \tag{18}$$

where

$$\hat{\mathbf{A}}(\mathbf{z}^{(i)}) = \begin{bmatrix} [\mathbf{W}(\mathbf{z}^{(i)})] & \begin{matrix} -\mathbf{G} \cdot \mathbf{a}^{(i)} \\ -\mathbf{G} \cdot \mathbf{b}^{(i)} \end{matrix} \\ \begin{matrix} \mathbf{B}\ \mathbf{0} \\ \mathbf{0}\ \mathbf{B} \end{matrix} & \begin{matrix} \mathbf{0} \\ \mathbf{0} \end{matrix} \\ (\mathbf{t}^{(i-1)})^T & \end{bmatrix},$$

$$\mathbf{W}(\mathbf{z}) = \begin{bmatrix} \mathbf{D} + \mathbf{V} - \lambda^{(i)}\mathbf{G} + \dfrac{\partial(\mathbf{E} + \mathbf{L})}{\partial \mathbf{a}}(\mathbf{z}) & \dfrac{\partial(\mathbf{E} + \mathbf{L})}{\partial \mathbf{b}}(\mathbf{z}) \\ \dfrac{\partial(\mathbf{K} + \mathbf{Q})}{\partial \mathbf{a}}(\mathbf{z}) & \mathbf{D} + \mathbf{V} - \lambda^{i}\mathbf{G} + \dfrac{\partial(\mathbf{K} + \mathbf{Q})}{\partial \mathbf{b}}(\mathbf{z}) \end{bmatrix}.$$

Note that as the number of collocation points is increasing, the matrix $\hat{\mathbf{A}}$ is going to be nearly singular or badly scaled since the ill-condition on the discretization matrix of the RBFCM-CM. Thus, if the condition number of $\hat{\mathbf{A}}$ is greater than a threshold, we suggest another small perturbation vector $\bar{\mathbf{d}}$ to be added in the diagonal entries of $\hat{\mathbf{A}}$ for the computational stability.

We implement the predictor-corrector continuation to approximate the energy level of the CNLSE by tracing its solution curve. We first determine the eigenvalues of the associate LSE. Then we use the first bifurcation $(0, \lambda_1)$ of LSE to predict the first solution curve branching of the CNLSE, and continuously traces the solution curve until it reaches the target point that satisfies the mass conservation constraint.

4. Numerical results

We examine the RBFCM-CM for solving the CNLSE Eq. (3) and investigate its performance for the mixture with continuation method to trace the solution curve. The first solution branches (**u**, **v**, λ) were numerically traced by using the predictor-corrector continuation method, where the perturbation vector **d** was chosen with $\|d\|_\infty = 5 \times 10^{-5}$. Here we inspect the superfluid density denoted by $|\Psi(\mathbf{x}, t)|^2 = |q(\mathbf{x})|^2 = u^2(\mathbf{x}) + v^2(\mathbf{x})$ when it satisfies the mass conservation constraint. All experiments were performed with MATLAB 2009B with double precision arithmetic on a PC with Intel Xeon Processor E5520 at 2.26 GHz .

We let the isotropic potential function $V(\mathbf{x}) = (x^2 + y^2)/2$, and the computational domain is $\Omega = (-12, 12)^2$. In order to obtain a round-shape figure with regular distribution in vortices, we choose $\mu = 100$. The finite element method (FEM) is implemented here using a Galerkin approximation under the piecewise bilinear elements. The stopping tolerance in Newton corrector is 10^{-10}.

Example 1: The RBFCM for the LSE

Consider a two-dimensional linear harmonic oscillator of the dimensionless form

$$-\frac{1}{2}\Delta u(\mathbf{x}) + V(\mathbf{x})u(\mathbf{x}) = \lambda u(\mathbf{x}), \qquad \mathbf{x} \in \Omega = \mathbb{R}^2 \tag{19}$$

with $\lim_{|\mathbf{x}| \to \infty} \mathbf{u}(\mathbf{x}) = 0$, where $V(\mathbf{x}) = (x^2 + y^2)/2$. By separation of variables, Eq. (19) is divided into two one-dimensional harmonic oscillator (1-D HO). In many quantum mechanics literatures, e.g. Landau (1977), the normalized eigenpairs of 1-D HO are given by

$$u_{mn}(x, y) = \frac{e^{-(x^2+y^2)/2}}{\sqrt{2^{m+n} m! n! \pi}} H_m(x) H_n(y), \qquad \lambda_{mn} = m + n + 1, \qquad m, n = 0, 1, 2, \ldots, \tag{20}$$

where $H_n(x) = (-1)^n e^{x^2} \frac{d^n}{dx^n} e^{-x^2}$ is the Hermite polynomial of order n. To measure the solution error, Huang (2010) denoted the normalized root mean square (RMS) for the error as

$$\mathrm{RMS}(e) = \frac{\sqrt{\Sigma_{i=1}^{N} e^2(\mathbf{x}_i)}}{\sqrt{N} \max_{1 \le i \le N} |u(\mathbf{x}_i)|}$$

where e is the error for the approximation of u. Tables 1 and 2 and Fig. 1 show the errors of the first eigenpair obtained from the FEM-CM and RBFCM-CM. The error of FEM-CM is decreasing in order of $O(h^2)$ while the RBFCM-CM with a constant shape parameter ($c = 1$) converges in an exponential order $O(\gamma^{h^{-1.15}})$ with the exponential base $\gamma \approx 0.89$.

Example 2: The selection of the shape parameters

The shape parameter is crucial for the success of using the RBFCM. The RBF performs the collocation method better than polynomials as the shape parameter exists (Huang *et al*. 2007, 2010). Here, we investigate the relation between the shape parameter and the error of the RBFCM-CM for the LSE. Table 3 shows the error of the RBFCM-CM on three uniform partitions: $N = 31 \times 31$, $41 \times$

Table 1 The convergence in order of O(h^q) (quadratic) by using the FEM-CM for the LSE

i	N	RMS	q
1	32 × 32	3.49*E*-2	–
2	64 × 64	8.77*E*-3	1.99
3	128 × 128	2.20*E*-3	2.00
4	256 × 256	5.49*E*-4	2.00
5	512 × 512	1.37*E*-4	2.00
6	1024 × 1024	3.41*E*-5	2.01

Table 2 The convergence in order of O (γ^{h^q}) by using the RBFCM-CM with a fixed shape parameter $c = 1$, $q = 1.15$, $\gamma \approx 0.89$ for the LSE

i	N	RMS	γ
1	31 × 31	0.11*E*-2	–
2	35 × 35	5.02*E*-4	0.903
3	41 × 41	1.39*E*-4	0.897
4	45 × 45	5.63*E*-5	0.894
5	51 × 51	1.40*E*-5	0.893
6	55 × 55	5.47*E*-6	0.893
7	61 × 61	1.31*E*-6	0.893
8	65 × 65	5.00*E*-7	0.894

Table 3 The RMS of errors vs. the shape parameter for the number of collocation points 31 × 31, 41 × 41 and 51 × 51

$N = 31 \times 31$		$N = 41 \times 41$		$N = 51 \times 51$	
c	RMS	c	RMS	c	RMS
1.5	1.74*E*-4	1.5	7.16*E*-6	1.5	2.14*E*-7
2.0	4.04*E*-5	2.0	6.77*E*-6	2.0	1.05*E*-8
2.5	1.23*E*-5	2.5	3.26*E*-8	2.5	2.71*E*-9
3.0	4.11*E*-6	3.0	3.26*E*-8	2.6	2.16*E*-9
3.5	1.04*E*-6	3.5	1.20*E*-8	2.7	1.72*E*-9
3.7	2.75*E*-7	3.7	8.46*E*-9	2.8	1.39*E*-9
3.78	**1.39*E*-7**	3.8	7.12*E*-9	2.9	1.28*E*-9
3.8	1.47*E*-7	3.9	6.14*E*-9	**3.0**	**1.02*E*-9**
4.0	5.44*E*-7	**4.0**	**5.73*E*-9**	3.1	1.55*E*-9
4.5	1.33*E*-6	4.1	8.35*E*-9	3.5	5.23*E*-8

41 and 51 × 51 with various shape parameters for the first eigenpair of Eq. (19). Fig. 2 shows that our results agree with Huang's (2007) results, and as c is increasing, the error is decreasing sharply until the critical value c_{cr}. However, around the critical value, the condition number of the discrete matrix $\hat{\mathbf{A}}$ of RBFCM-CM might become extremely large, and this increases the difficulty in solving the linear system.

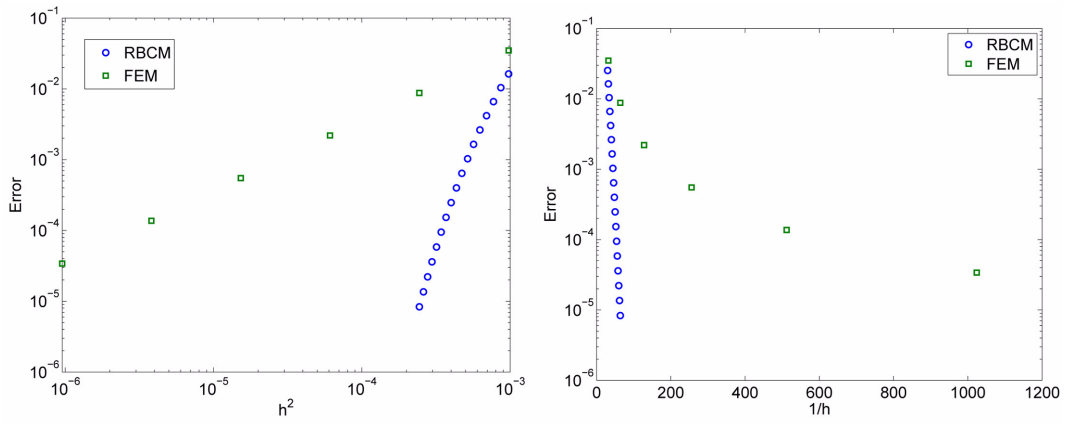

(a) The error vs. h^2. (b) The error vs. $1/h$.

Fig. 1 The curves for the convergent rates for the FEM-CM and RBFCM-CM with various grid-sizes for LSE

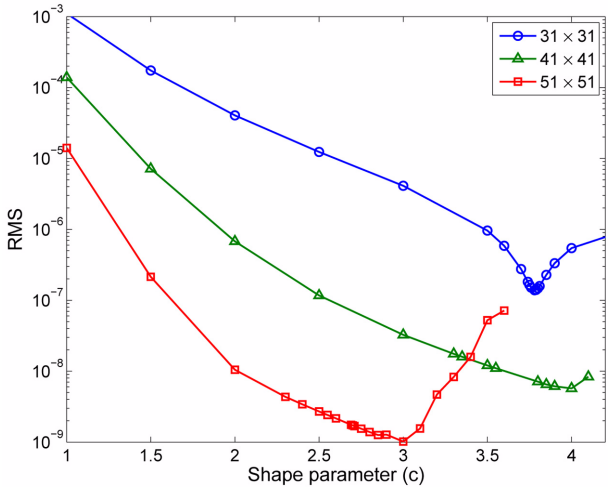

Fig. 2 The RMS of error curves vs. shape parameter for the number of collocation points 31×31, 41×41 and 51×51

Example 3: The ground state solutions of a rotating BEC with vortex lattices

In this example, we study the RBFCM-CM for solving CNLSE with various angular momentum rotation term ω. We fix the shape parameter $c = 1.1$. The computational grid in the RBFCM-CM is only limited on 51×51 collocation points, which is far less than the required number in FEM. The computational grid in the FEM-CM is 128×128 to ensure the solution quality for the comparison. Figs. 3-6 show the 3D plots and contours of the superfluid densities obtained from both the FEM-CM and the RBFCM-CM for $\omega = 0.5$, 0.7, 0.9 and 0.95, and the number of vortex lattices is increasing up to 20. We find that the solutions of the RBFCM-CM are very good qualitative agreement in the FEM-CM for studying the complexity of vortex lattices in rotating BEC.

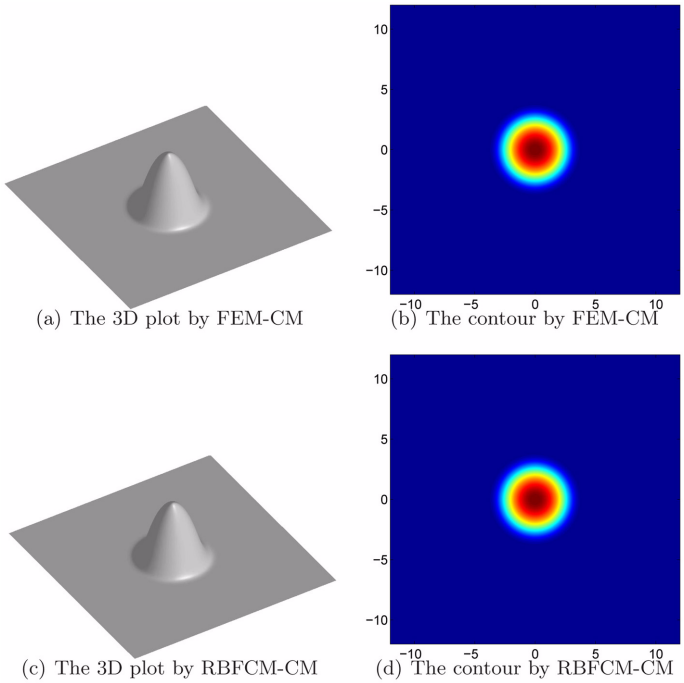

Fig. 3 The 3D plots of the superfluid density for $\omega = 0.5$ and the contours by the FEM-CM and RBFCM-CM. There is no vortex lattice when $\omega = 0.5$

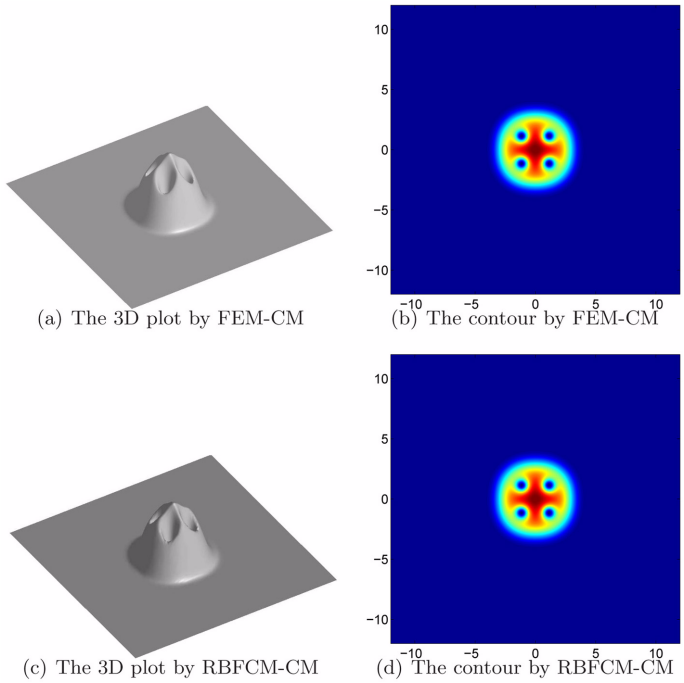

Fig. 4 The 3D plots of the numerical solutions for the superfluid density for $\omega = 0.7$ and the contours by the FEM-CM and RBFCM-CM. Both contain 4 vortex lattices

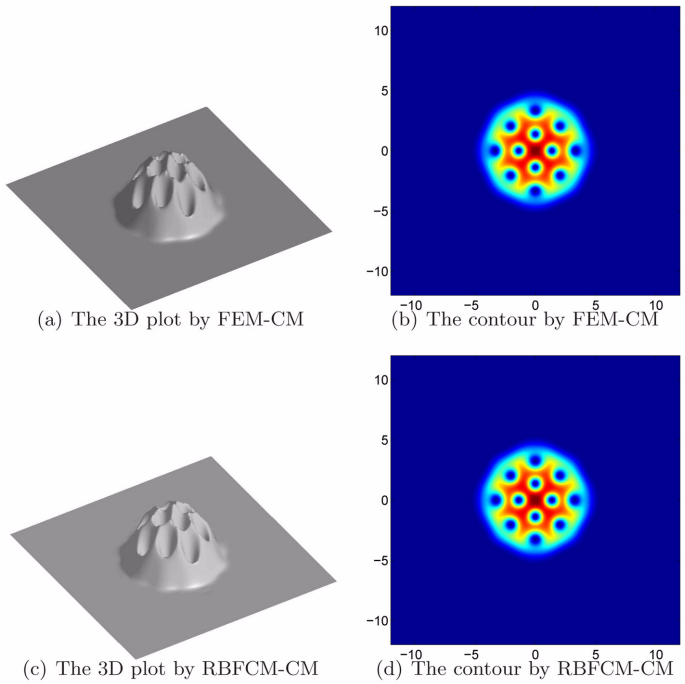

(a) The 3D plot by FEM-CM (b) The contour by FEM-CM

(c) The 3D plot by RBFCM-CM (d) The contour by RBFCM-CM

Fig. 5 The 3D plots of the superfluid density for $\omega = 0.9$ and the contours by the FEM-CM and RBFCM-CM. Both contain 12 vortex lattices

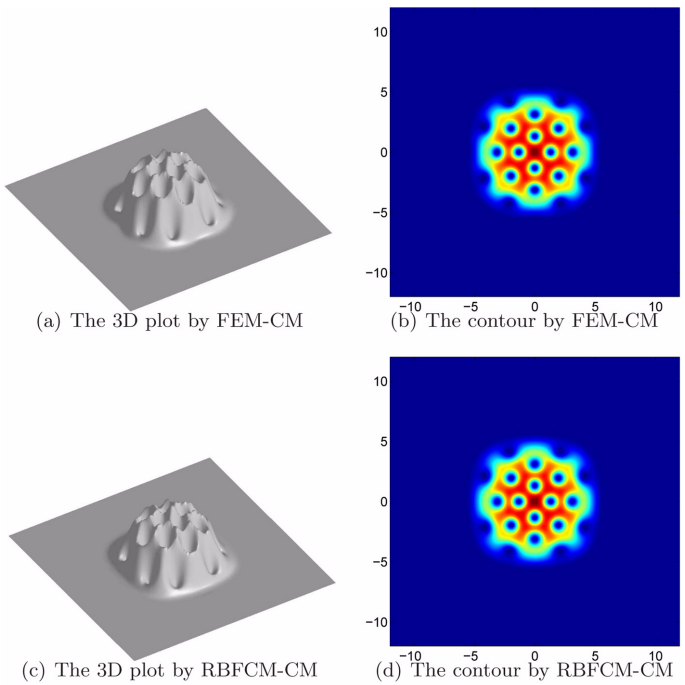

(a) The 3D plot by FEM-CM (b) The contour by FEM-CM

(c) The 3D plot by RBFCM-CM (d) The contour by RBFCM-CM

Fig. 6 The 3D plots of the superfluid density for $\omega = 0.95$ and the contours by the FEM-CM and RBFCM-CM. Both contain 20 vortex lattices

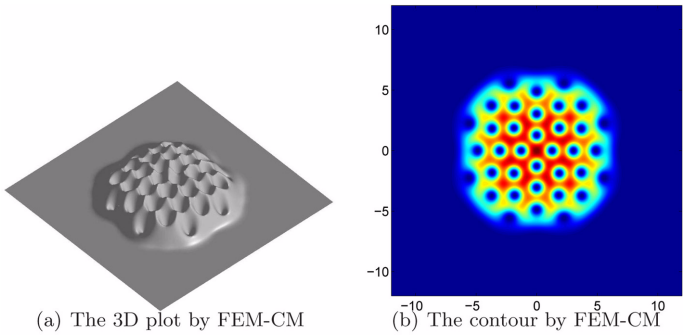

(a) The 3D plot by FEM-CM (b) The contour by FEM-CM

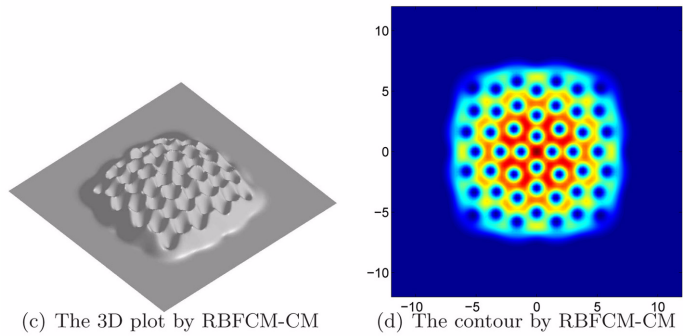

(c) The 3D plot by RBFCM-CM (d) The contour by RBFCM-CM

Fig. 7 The 3D plots of the superfluid density for $\omega = 0.99$ and the contours. The superfluid densities by the RBFCM-CM and FEM-CM contain 48 and 36 vortex lattices, respectively

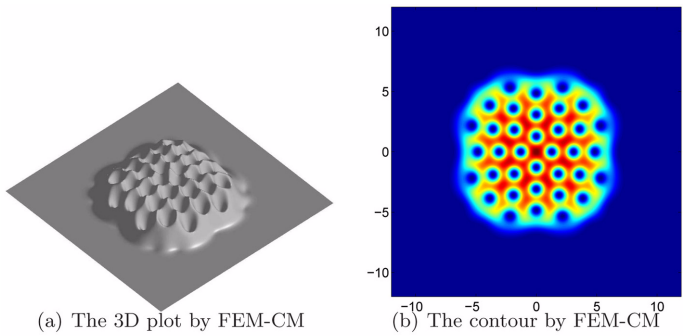

(a) The 3D plot by FEM-CM (b) The contour by FEM-CM

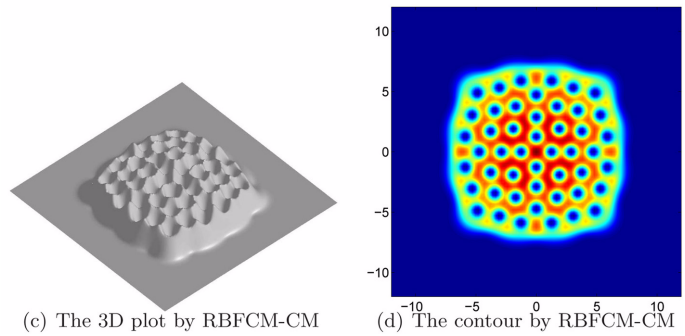

(c) The 3D plot by RBFCM-CM (d) The contour by RBFCM-CM

Fig. 8 The 3D plots of the superfluid density for $\omega = 0.995$ and the contours. The superfluid densities by the RBFCM-CM and FEM-CM contain 48 and 36 vortex lattices, respectively

Example 4: The ground state solutions of a fast rotating BEC

This example exhibits the capability of the RBFCM-CM for solving a fast rotating BEC when $\omega \geq 0.99$. When implementing the RBFCM-CM, we let the shape parameter $c = 1.1$, and let the computational points be 81×81. We let the computation grids 256×256 for the FEM-CM with the bilinear element. Figs. 7-8 show the 3D plots and the contours of the superfluid densities obtained from both the FEM-CM and the RBFCM-CM for $\omega = 0.99$ and 0.995. The number of vortex lattices for two cases is 48 by the RBFCM-CM and 36 by the FEM-CM. Hence, the RBFCM-CM using only coarsen points excels the FEM-CM with finer grids.

5. Conclusions

We have studied the RBFCM for numerical solutions of a coupled nonlinear Schrödinger equations (CNLSE) for modeling a rotating BEC. That is, the RBFCM is incorporated with the continuation method to trace the solutions of the eigenvalue problems. We show that the RBFCM-CM converges quickly in an exponential rate for the LSE, and our results also depict the advantage of the RBFCM-CM for using fewer grid points for the discretization than those the FEM-CM requires. Furthermore, as angular momentum rotation term ω approaches to 1, the number of vortex lattices will be generated more, and this increases the difficulty for determining the number of collocation points. In the future, we plan to extend the idea to develop a novel RBFCM with a variable shape parameter for computing a rotating BEC with many vortex latices or in optical lattices.

Acknowledgements

The authors acknowledge support by the National Science Council of Taiwan through Project NSC 98-2115-M-005-005. We also thank Mr. Y.-C. Lin of the National Chung-Hsing University for his contributions in developing the FEM-continuation software for rotating BEC. The authors also thank the anonymous referees for their kind comments and valuable suggestions.

References

Aftalion, A. and Danaila, L. (2002), "Three-dimensional vortex configurations in a rotating Bose Einstein condensate", *Phys. Rev. Lett*., **68**(2), 023603.

Allgower, E. and Georg, K. (1990), *Numerical continuation method: An introduction*, Springer-Verlag, New York.

Anderson, M.H., Ensher, J.R., Matthews, M.R., Wieman, C.E. and Cornell, E.A. (1995), "Observation of Bose-Einstein condensation in a dilute atomic vapor", *Science*, **269**(5221), 198-201.

Baksmaty, L.O., Liu, Y., Landmanc, U., Bigelowd, N.P. and Pu, H. (2009), "Numerical exploration of vortex matter in Bose-Einstein condensates", *Math. Comput. Simulat*., **80**(1), 131-138.

Bao, W. and Wang, H. (2006), "An efficient and spectrally accurate numerical method for computing dynamics of rotating Bose-Einstein condensates", *J. Comput. Phys*., **217**(2), 612-626.

Butts, D.A. and Rokhsar, D.S. (1999), "Predicted signatures of rotating Bose-Einstein condensates", *Nature*, **397**(6717), 327-329.

Chang, S.L. and Chien, C.S. (2007), "Adaptive continuation algorithms for computing energy levels of rotating Bose-Einstein condensate", *Comput. Phys. Commun*., **177**(9), 707-719.
Davis, K.B., Mewes, M.O., Andrews, M.R., van Druten, N.J., Durfee, D.S., Kurn, D.M., and Ketterle, W. (1995), "Bose-Einstein condensation in a gas of sodium atoms", *Phys. Rev. Lett*., **75**(22), 3969-3973.
Fasshauer, G.E. (2002), "Newton iteration with multiquadrics for the solution of nonlinear PDEs", *Comput. Math. Appl*., **43**(3-5), 423-438.
Ferreira, A.J.M., Roque, C.M.C., Jorge, R.M.N. and Kansa, E.J. (2005), "Static deformations and vibration analysis of composite and sandwich plates using a layerwise theory and multiquadrics discretization", *Eng. Anal. Bound. Elem.*, **29**(12), 1104-1114.
Fornberg, B. and Piret, C. (2008), "On choosing a radial basis function and a shape parameter when solving a convective PDE on a sphere", *J. Comput. Phys*., **227**(5), 2758-2780.
Gross, E.P. (1961), "Structure of a quantized vortex in boson systems", *Nuovo. Cimento*., **20**(3), 454-477.
Hardy, R.L. (1971), "Multiquadric equations of topography and other irregular surfaces", *J. Geophys. Res*., **76**(8), 1905-1915.
Hu, H.Y., Lai, C.K. and Chen, J.S. (2009), "A study on convergence and complexity of reproducing kernel collocation method", *Interact. Multiscale Mech*., **2**(3), 295-319.
Hu, H.Y., Li, Z.C. and Cheng, A.H.D. (2005), "Radial basis collocation methods for elliptic boundary value problems", *Comput. Math. Appl*., **50**(1-2), 289-320.
Huang, C.S., Lee, C.F. and Cheng, A.H.D. (2007), "Error estimate, optimal shape factor, and high precision computation of multiquadric collocation method", *Eng. Anal. Bound. Elem*., **31**(7), 614-623.
Huang, C.S., Yen, H.D. and Cheng, A.H.D. (2010), "On the increasingly flat radial basis function and optimal shape parameter for the solution of elliptic PDEs", *Eng. Anal. Bound. Elem*., **34**(9), 802-809.
Kansa, E.J. (1990), "Multiquadrics -a scattered data approximation scheme with applications to computational fluiddynamics -I.", *Comput. Math. Appl*., **19**(8-9), 127-145.
Kindelan, M., Bernal, F., Pedro Gonzalez-Rodriguez, P. and Moscoso, M. (2010), "Application of the RBF meshless method to the solution of the radiative transport equation", *J. Comput. Phys*., **229**(5), 1897-1908.
Landau, L.D. and Lifshitz, E.M. (1977), *Quantum mechanics, Non-relativistic Theory*, Pergamon Press.
Matveenko, S.I., Kovrizhin, D., Ouvry, S. and Shlyapnikov, G.V. (2009), "Vortex structures in rotating Bose-Einstein condensates", *Phys. Rev. A*, **80**(6), 063621.
Micchelli, C. (1986), "Interpolation of scattered data: Distance matrices and conditionally positive definite functions", *Constr. Approx*., **2**(1), 11-22.
Pitaevskii, L.P. (1961), "Vortex lines in an imperfect Bose gas", *Soviet Phys. JETP*., **13**(2), 451-454.
Wang, L., Chen, J.S. and Hu, H.Y. (2009), "Radial basis collocation method for dynamic analysis of axially moving beams", *Interact. Multiscale Mech*., **2**(4), 333-352.